2-1986

Altering the Photorefractive Properties of BaTiO3 by Reduction and Oxidation at 650 °C

Stephen Ducharme
University of Nebraska at Lincoln, sducharme1@unl.edu

Jack Feinberg
University of Southern California

Altering the photorefractive properties of $BaTiO_3$ by reduction and oxidation at 650°C

Stephen Ducharme and Jack Feinberg

Department of Physics, University of Southern California, University Park, Los Angeles, California 90089-0484

Received July 30, 1985; accepted October 7, 1985

The photorefractive properties of a nominally pure single crystal of $BaTiO_3$ were altered by treating the crystal at 650°C in oxygen at different partial pressures. Treatment altered the effective density of photorefractive charge carriers in the crystal and could convert an inactive crystal into an active one. Treatment at low oxygen pressure (reduction) decreased the temperature of the tetragonal-to-cubic phase transition of the crystal and also decreased the measured optical band gap, implying that oxygen vacancies had been introduced into the bulk crystal. These oxygen vacancies are associated with negative photorefractive charge donors. Either hole transport or electron transport dominated, depending on whether the partial pressure of oxygen was greater than or less than ½ atm during treatment. The competing roles of electrons and holes are discussed.

1. INTRODUCTION

Barium titanate ($BaTiO_3$) is a highly nonlinear optical material, which has been used for optical phase conjugation,[1] image processing,[2] and laser resonators.[3–6] The optical nonlinearity in $BaTiO_3$ is due to the photorefractive effect, in which nonuniform illumination redistributes charges in the crystal, causing a semipermanent change in the crystal's refractive index. However, because the charges originate from defects or impurities, both the magnitude and the speed of the photorefractive effect can vary from one sample of $BaTiO_3$ to another; in some $BaTiO_3$ samples the optical nonlinearity is strong, whereas in others the nonlinearity is very weak.

We report experiments in which we have deliberately altered the density of photorefractive charges, and the relative contribution of electrons and holes to photorefraction, by exposing a nominally pure single crystal of $BaTiO_3$ to various partial pressures of oxygen at a temperature of 650°C. We were able to change a crystal from being inactive to active and to change the dominant charge carrier from holes to electrons and back to holes again.

In Section 2 we outline the predictions of two current models of a photorefractive material as a compensated semiconductor. The first model is based on hopping transport as proposed by Feinberg *et al.*[7] The second is based on band conduction and is essentially that of Kukhtarev *et al.*,[8] but it includes the competition of holes and electrons as described by Orlowski and Kratzig[9] and further refined by Klein and Valley.[10] The hopping model has been generalized to large hopping distances by Mullen and Hellwarth,[11] and here we generalize the hopping model further to include the competing roles of electron and hole photoconduction (see Appendix A). The predictions of the hopping and the band-conduction models are the same for the experimental tests performed here.

Our experimental results are presented in Section 3 and are in reasonable agreement with theory if we identify the photorefractive charge donors as (1) singly ionized oxygen vacancies or (2) donor complexes composed of an oxygen vacancy adjacent to a trace impurity. We show that the density of oxygen vacancies determines the density of photorefractive donors in $BaTiO_3$. Our results also demonstrate the competition of electron and hole transport in $BaTiO_3$.

2. THEORY

A. Steady-State Space-Charge Field

Consider movable charges (either electrons or holes) occupying sites distributed uniformly throughout the material. The sites might be impurity atoms or point defects. A site can be occupied either by an electron or a hole. Figure 1 shows how the movable charges will be redistributed by diffusion when illuminated nonuniformly. If *electrons* diffuse away from the illumination, then the resulting electrostatic field will be directed *away* from the light and toward the dark regions, as shown in Fig. 1(a). If *holes* diffuse away from the illumination, then the space-charge field will be directed *toward* the light regions, as in Fig. 1(b). In general both holes and electrons are movable, and their space-charge fields tend to cancel.

A steady-state charge distribution is obtained when the diffusive force due to nonuniform illumination is balanced by the electrostatic field produced by the displaced charges themselves. In a crystal lacking inversion symmetry, this space-charge field causes a first-order distortion of the crystal lattice, thus altering the crystal's refractive index by the linear electro-optic (Pockels) effect. This refractive-index change can be monitored with another optical beam. More detailed descriptions of the formation of this protorefractive index change are found in Refs. 1, 7, and 8.

If the material is a semiconductor with only *one* kind of deep defect site (e.g., an impurity atom or a point defect), then all these sites are full, no charges can be redistributed, and there is no photorefractive effect. However, if one adds another set of sites that *partially* deplete the first set, then a redistribution is possible, and a photorefractive effect may be observed. Figure 2(a) shows an example in which the

0740-3224/86/020283-10$02.00

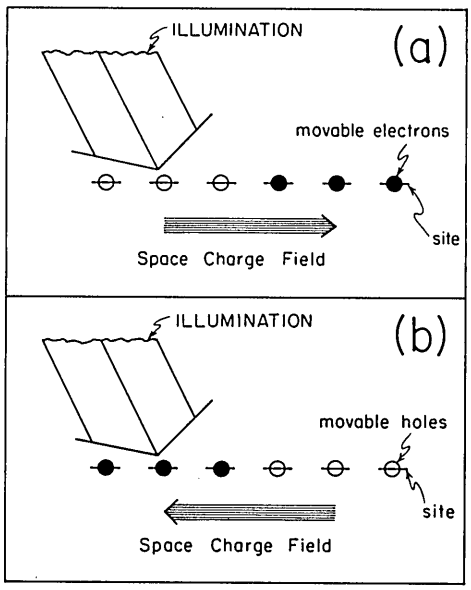

Fig. 1. Rearrangement of charges by light in a photorefractive material. In (a) electrons have diffused [and in (b) holes have diffused] away from the illuminated region. In general, both processes may occur simultaneously producing opposite space-charge fields as shown. The space-charge field produced by electron migration affects the migration of both electrons and holes, and vice versa.

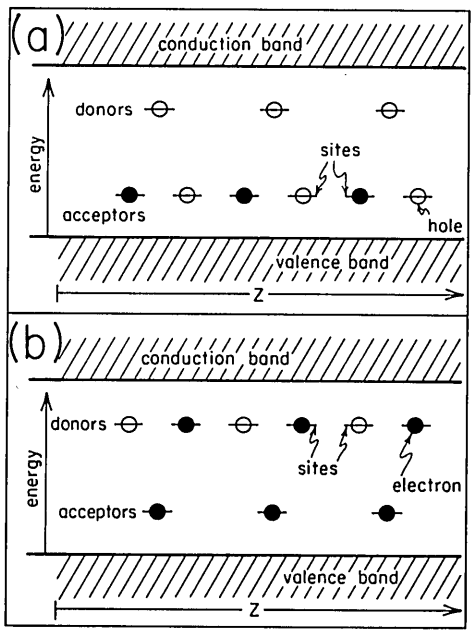

Fig. 2. Schematic of donor and acceptor levels in a photorefractive semiconductor. In (a) the density of acceptors exceeds the density of donors, and holes can be redistributed by light among the acceptor sites. In (b) the density of donors exceeds the density of acceptors, and electrons can be redistributed by light among the donor sites.

acceptor sites, with number density N_A, are partially filled by electrons transfered from the donor sites, which have number density N_D. In this example the acceptor sites are more numerous ($N_A > N_D$). (We assume that the donor sites remain empty even in the presence of light.[12]) The remaining N_A–N_D *holes* may then be redistributed by light among the acceptor sites. Figure 2(b) shows the opposite case, in which the donor sites are more numerous ($N_D > N_A$) and the acceptor sites are full (and remain full[12]), and the remaining N_D–N_A *electrons* may then be redistributed by light among the donor sites.

Note that charge transport is possible by both electron and hole conduction in either Fig. 2(a) or 2(b). The electron and hole contributions to the photoconductivity add. In contrast, the electron and hole contributions to the photorefractive space-charge electric field compete and reduce this field, as discussed later.

There are currently two models describing photorefractive charge transport. The band model[8] is a three-step process shown for electron transport in Fig. 3(a): (1) photoionization of a carrier bound at a defect site; (2) drift and diffusion of the carrier through the conduction band; and (3) recombination at a new defect site. The hopping model[7] considers single hops (photoassisted tunneling) between sites, as shown in Fig. 3(b). The two models predict the same results as long as the electron (or hole) recombination time is short compared to any optical transients and the relative charge modulation is small. The experiments reported here do not distinguish between the two models.

Consider light modulated sinusoidally in space with spatial frequency k is incident upon the crystal (for example, the interference fringes of two intersecting coherent optical beams) according to

$$I(z) = I_0\{1 + \mathrm{Re}[m \exp(ikz)]\}. \tag{1}$$

For small modulation ($|m| \ll 1$), the resulting space-charge field will be

$$E(z) = \mathrm{Re}[E_{sc} \exp(ikz)], \tag{2}$$

where

$$E_{sc} \equiv [iRmk_BT/e][k/(1 + (k/k_0)^2)], \tag{3a}$$

$$k_0^2 \equiv N_{pr}e^2/(\epsilon\epsilon_0 k_B T), \tag{3b}$$

$$N_{pr} \equiv N_D(1 - N_D/N_A) \quad N_A > N_D$$
$$\equiv N_A(1 - N_A/N_D) \quad N_D > N_A, \tag{3c}$$

$$R \equiv (\sigma_+ - \sigma_-)/(\sigma_+ + \sigma_- + \sigma_d), \tag{3d}$$

according to either the band[8–10] or the hopping (see Refs. 7, 11, and Appendix A) model, where k_B is Boltzmann's constant, T is the lattice temperature, ϵ is the (dimensionless) dielectric constant, ϵ_0 is the permittivity of free space, e is the

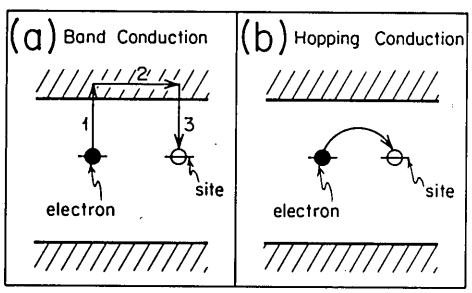

Fig. 3. Two mechanisms of photoconduction. (a) Band conduction is a three-step process: (1) thermal ionization or photoionization, (2) drift or diffusion within the band, (3) recombination at an empty site. (b) Hopping is a one-step process of thermal-assisted or photoassisted tunneling. These examples show electron conduction; hole conduction is also possible.

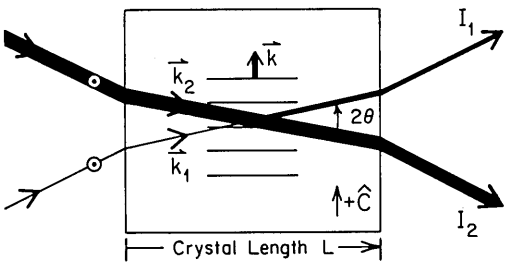

Fig. 4. Beam geometry for two-beam energy coupling experiments. $\mathbf{k}_1$ and $\mathbf{k}_2$ are the optical wave vectors of the beams in the crystal. The $+c$ crystal axis is oriented parallel to the grating wave vector $\mathbf{k} = \mathbf{k}_1 - \mathbf{k}_2$. If hole photoconduction is dominant, then beam number 1 experiences gain, as indicated schematically on the figure by the width of the beam. The intersection angle in the crystal is 2θ. Both beams are polarized perpendicular to the plane of the figure and are ordinary rays.

absolute value of the charge of an electron (or hole), and N_{pr} is the effective density of photorefractive charge carriers.

The parameter R weighs the photorefractive contributions of hole photoconductivity σ_+, electron photoconductivity σ_-, and dark conductivity σ_d. Equation (2) and expression (3) assume that steady state has been reached, the charge-density modulation is small ($|m| \ll 1$), there is no applied or photovoltaic dc electric field, and the distance traveled by a movable charge per absorbed photon is small compared to the grating spacing. (This last restriction on the carrier lifetime in the band model, and on the hopping length in the hopping model, can be removed if necessary, as in Refs. 8 and 11 and in Appendix A.)

The space-charge field $E(z)$ of Eq. (2) creates a photorefractive-index variation $\Delta n(z)$ given by

$$\Delta n(z) = -(1/2)n^3 r_{\text{eff}} E(z), \tag{4}$$

where n is the index of refraction and r_{eff} is the effective Pockels coefficient of the crystal. Note that there is a 90° phase shift between refractive-index pattern $\Delta n(z)$ and the optical intensity pattern $I(z)$ owing to the factor of i in expression 3(a).

The effective density of photorefractive charge carriers N_{pr} and the relative contribution of electron and hole photoconductivities R can be determined by two-beam energy-coupling experiments.

B. Two-Beam Energy Coupling

Two coherent optical beams intersecting in a photorefractive material will, in general, transfer energy from one beam to the other. The photorefractive index pattern generated by the two beams acts as a volume diffraction grating and partially Bragg deflects each beam. One deflected beam adds constructively and the other deflected beam adds destructively to the transmitted beams (depending to the direction of the c axis of the crystal), causing a net transfer in energy from one beam to the other, as shown in Fig. 4. The direction of energy transfer relative to the c axis reveals the *sign* of the dominant photorefractive charge carrier. The variation in the magnitude of energy transfer with beam crossing angle yields the effective *density* of photorefractive charge carriers N_{pr}.[7]

Let the two optical beams have transmitted intensities $I_1 \ll I_2$ with wave vectors $\mathbf{k}_1$ and $\mathbf{k}_2$, respectively, in the crystal. Choose the direction of the c axis so that the weaker beam (number 1) experiences gain. If the stronger beam is negligibly depleted by the interaction, then the weaker beam will experience an exponential increase in intensity along its direction of propagation:

$$\frac{I_1 \text{ (with coupling)}}{I_1 \text{ (without coupling)}} = \exp(gL_1), \tag{5}$$

where L_1 is the interaction length along beam 1. The exponential power gain coefficient g per unit length is[7]

$$g = \frac{R\delta k/(n\omega/c)}{[1 + (k/k_0)^2]}, \tag{6}$$

where ω is the optical frequency. For $I_1 \ll I_2$ the gain g is independent of the intensity of either beam. The spatial frequency k of the grating is given by

$$k = (2n\omega/c)\sin\theta, \tag{7}$$

and 2θ is the crossing angle of the writing beams inside the crystal (see Fig. 4). In Eq. (6), the quantity

$$\delta \equiv n^4(\omega/c)^2(r_{\text{eff}}k_B T/e) \tag{8}$$

is the intrinsic photorefractive coupling gain. Note that δ, which has units of inverse length, depends only on properties of the crystal lattice such as the Pockels coefficient, the index of refraction, and the temperature and not on the density or transport properties of the photorefractive charges nor on the spatial frequency k.

By measuring the variation of the two-beam coupling gain g with grating wave vector $\mathbf{k}$, both R and k_0^2 can be determined. The parameter R measures the competition between holes and electrons in forming the space-charge field. The parameter k_0^2 is proportional to the effective density of photorefractive charges. In the following section we describe two-beam energy-coupling experiments to measure these quantities.

3. EXPERIMENT RESULTS

A. Crystal Treatment

The $BaTiO_3$ crystal measured 0.37 cm × 0.42 cm × 0.42 cm with the c axis parallel to the shortest dimension. The crystal was grown from a top-seeded solution by Sanders Associates and, as grown, the sample was almost inactive photorefractively. The sample was first characterized by two-beam coupling and bulk absorption measurements and then repeatedly treated and recharacterized. For treatment the sample was placed in a 2.54-cm fused-quartz process tube inside a tube furnace and exposed in separate runs to various partial pressures of O_2 at 650°C for 36 h. The temperature of the sample was controlled with a microprocessor to follow the heating and cooling sequence shown in Fig. 5 with an accuracy of 0.5% and a stability of 0.2%. During heating and cooling the temperature was changed at rates not exceeding 33°C per hour, and near the tetragonal-to-cubic phase transition (at about 125°C) the rate was decreased to 4°C per hour to prevent stress fractures.

A total of three treatments were performed with the following flowing atmospheres (in chronological order):

(1) $\sim 10^{-6}$ atm of O_2 in ultrahigh-purity (99.999%) argon at atmospheric pressure,

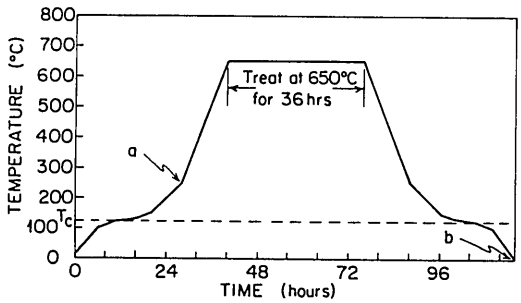

Fig. 5. Oven program temperature versus time for a typical $BaTiO_3$ treatment cycle. Flow of the oxygen-containing gas was started at the time marked a and stopped at b. The tetragonal-to-cubic phase transition of the crystal occurs at $T_c \approx 125°C$ in $BaTiO_3$.

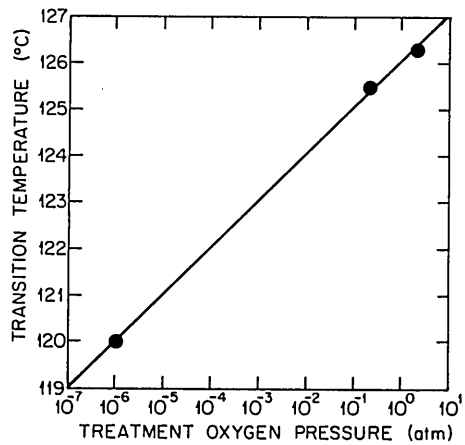

Fig. 6. Tetragonal-to-cubic phase transition temperature T_c of the $BaTiO_3$ crystal versus the oxygen partial pressure of the most recent treatment.

(2) ordinary air (~0.2 atm O_2, including Los Angeles smog),

(3) 2 atm of medicinal grade (99.99%) oxygen.

B. Poling the Crystal

After each treatment, the $BaTiO_3$ crystal was cooled to room temperature, removed from the furnace, and repoled as follows. The crystal was placed between two chrome-plated brass electrodes and held with light spring pressure. The assembly was immersed in silicon oil and slowly heated to ~0.5°C *above* the tetragonal-to-cubic phase-transition temperature, which occurred near 125°C. The rate of temperature change did not exceed 20°C per hour during heating and was less than 2°C per hour when near the transition. The transition temperature was determined by two methods. In the first, the capacitance of the crystal was monitored with a capacitance bridge, and the capacitance was observed to increase sharply from ~7 pF to a maximum >50 pF at the transition temperature. The second method consisted of monitoring the visual appearance of the crystal between crossed polarizers as it was slowly heated; striking colors suddenly appeared as the crystal abruptly changed from its tetragonal to its cubic phase. After the transition had occurred, a dc electric field of ~250 V/mm was applied (gradually, over a few minutes), and the crystal was slowly cooled (overnight) to room temperature, after which the applied electric field was removed.

Figure 6 shows the temperature of the tetragonal-to-cubic phase transition (measured during poling by the visual method described above) versus the oxygen partial pressure during the crystal's most recent treatment. The transition temperature decreased as the treatment oxygen pressure was decreased. This decrease was caused by oxygen *defects*' being introduced into the crystal as the treatment oxygen pressure was reduced, as previously demonstrated in experiments with polycrystalline[13] and flux-grown[14] single crystals. The actual oxygen-vacancy density is not known, but the number of vacancies should increase monotonically as the treatment oxygen pressure is reduced.

C. Absorption Spectra

Figure 7 shows the absorption spectrum of the crystal (at 22°C) as grown and after each oxygen treatment, as measured with a Beckman DK2A spectrophotometer. Two features stand out: First, a broad absorption plateau is seen to extend throughout the visible spectrum from about 800 nm (1.6 eV) to the band edge at 410 nm (3 eV). Note that this absorption plateau is smaller in the as-grown crystal and also in the crystal that had been treated with 0.2 atm of O_2. Second, the band edge at approximately 410 nm shifted to longer wavelengths as the treatment oxygen pressure was reduced, indicating that the band gap was decreased or softened by the presence of oxygen defects. This agrees with Ref. 14 and with the corresponding decrease in the transition temperature observed in Fig. 7.

An additional narrow absorption line was observed in the infrared at 2870 nm (0.43 eV) on an otherwise featureless background. Its width was ~12 nm, and its height was 0.35 cm^{-1} for the crystal as grown, 0.11 cm^{-1} after treating in 10^{-6} atm of oxygen, and 0.15 cm^{-1} after treating in 2.0 atm. This absorption may be caused by a defect or impurity color center. If the onset of the absorption plateau at 1.6 eV (~800 nm) in Fig. 7 is taken to be the ionization threshold of a hydrogenlike color center, then the absorption at 0.43 eV could result from the $n = 1$ to $n = 2$ absorption line at an expected energy of (1/4) × 1.6 eV = 0.4 eV.

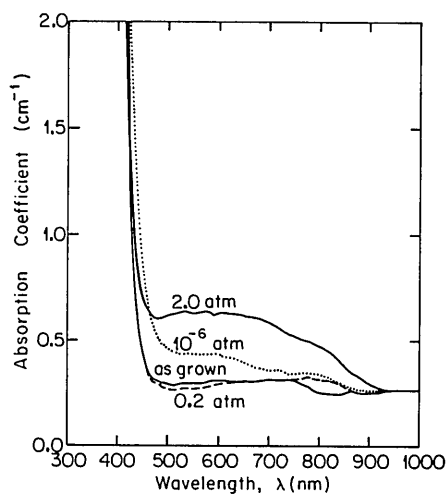

Fig. 7. Bulk optical absorption coefficient versus wavelength for the $BaTiO_3$ crystal as grown and after each treatment. Note that the absorption plateau in the visible portion of the spectrum is diminished for the crystal as grown and also after treatment with 0.2 atm of oxygen.

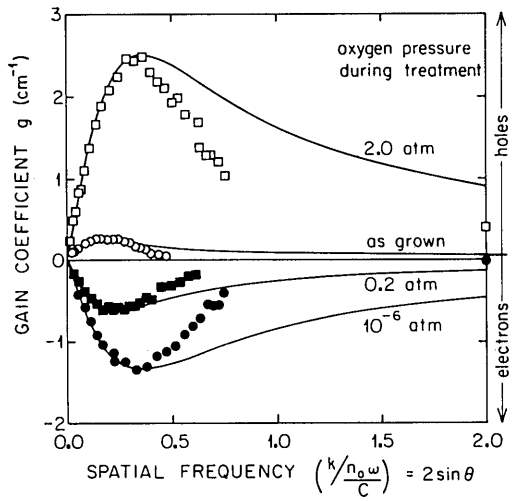

Fig. 8. Two-beam energy coupling gain coefficient g versus grating spatial frequency (in units of optical wave vector $n_0\omega/c$), for the $BaTiO_3$ crystal after treatment with various oxygen partial pressures. As grown (open circles); 10^{-6} atm (filled circles); 0.2 atm (filled squares); 2 atm (open squares). Note that the coupling gain coefficient switches sign between the oxidized crystal (2 atm of O_2) and the reduced crystal (10^{-6} atm of O_2), as discussed in the text. The curves are theoretical fits to Eq. (6).

D. Two-Beam Energy Coupling

Two-beam energy-coupling experiments were performed with an argon-ion laser operating at 514.5 nm on a single longitudinal TEM_{00} mode. Two coherent Gaussian beams with intensities $I_1 = 2.4 \times 10^{-5}$ W/cm^2 and $I_2 = 1.4 \times 10^{-1}$ W/cm^2 and diameters of 3 mm were aligned so that the direction of the grating wave vector $\mathbf{k}$ was parallel to the c axis of the $BaTiO_3$ crystal. The beams were polarized perpendicular to the plane of intersection and so were ordinary rays in the crystal. (Extraordinary rays cause experimental problems: they produce a much larger coupling strength, which can cause significant depletion of the stronger beam. Also, the effective Pockels coefficient r_{eff} depends more sensitively on the alignment of the crystal with respect to the optical beams for extraordinary rays than for ordinary rays.[15])

The increase in the transmitted intensity of the weak beam I_1 due to the presence of the strong beam I_2 was measured, and the small-signal gain coefficient g was determined from Eq. (5). The magnitude of the grating wave vector $k \equiv |\mathbf{k}_1 - \mathbf{k}_2| = (2n_0\omega/c)\sin\theta$ was varied by changing the crossing angle 2θ of the beams in the crystal. A plot of the measured gain coefficient g versus grating spatial frequency k is shown in Fig. 8, along with theoretical fits using Eq. (6) and the following constants: $r_{\text{eff}} = r_{13} = 14 \times 10^{-12}$ m/V (the unclamped Pockels coefficient for ordinary rays[16]), $n_0 = 2.488$, $\epsilon = 150$, $T = 22°C$, $\lambda = 514.5$ nm, $L = 0.42$ cm, $L_1 = L/\cos\theta$, and hence $\delta = 20$ cm^{-1}.

The energy-coupling curves of Fig. 8 are seen to grow linearly with small k, reach a maximum at $k = k_0$, and then decrease for large k. The theoretical fits have two adjustable parameters: k_0 and R. The value of k_0 is controlled by the effective density of photorefractive charges N_{pr} [Eq. (3b)]; therefore the location of the energy-coupling peak gives the effective charge density. The parameter R is the relative contribution of electron and hole photoconductivities [Eq. (3d)] and is found from the slope at small k of each of the curves of Fig. 8. The sign of R determines the sign of the coupling coefficient g: it is positive for hole-dominated photoconduction and negative for electron-dominated photoconduction. When the crystal exhibited hole-dominated photoconduction it was oriented as shown in Fig. 4, with the c-axis direction along $\mathbf{k}$. When the crystal exhibited electron-dominated photoconduction it had to be rotated 180° (making the $+c$-axis direction *opposite* $\mathbf{k}$), so that the weak beam I_1 would still increase in the presence of the strong beam I_2, and pump depletion could be avoided. The data and the theoretical curves of Fig. 8 agree except at high spatial frequencies ($k \gg k_0$), where the measured gain is noticeably less than predicted by theory. The origin of this disagreement is not known.

E. Effective Density of Photorefractive Charge Carriers

Figure 9 is a plot of the effective density of photorefractive charge carriers N_{pr} determined from the two-beam coupling data versus the partial pressure of oxygen during treatment. Changing the treatment oxygen pressure drastically altered N_{pr}: After treatment at the small oxygen pressures (10^{-6} atm and 0.2 atm) the density of acceptors exceeded the density of donors ($N_A > N_D$); and after treatment at the large oxygen pressure (2.0 atm) the situation was reversed ($N_D > N_A$). The effective treatment oxygen pressure for the as-grown crystal is unknown; we assume that it lies between the 0.2- and 2.0-atm data points (indicated by the error bars in Fig. 9).[17] According to Eq. (3c), N_{pr} should vanish if $N_D = N_A$, because the donor sites would be completely empty and the acceptors would be completely full, and no redistribution of the charges would be possible. The data of Fig. 9 imply that N_{pr} would vanish if this crystal were treated in about 0.5 atm of oxygen at 650°C. We note that the broad absorption plateaus of Fig. 7 are also smallest after treatment near this pressure (the as-grown and the 0.2-atm data), indicating that this broad absorption may be associated with N_{pr}.

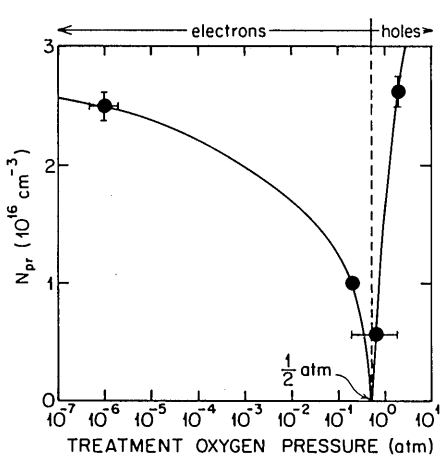

Fig. 9. The density of photorefractive charge carriers N_{pr} versus the oxygen partial pressure of the most recent treatment. The effective oxygen pressure for the crystal as grown is unknown but is assumed to lie in the region indicated by the error bars, as discussed in the text. The solid line is a qualitative guide.

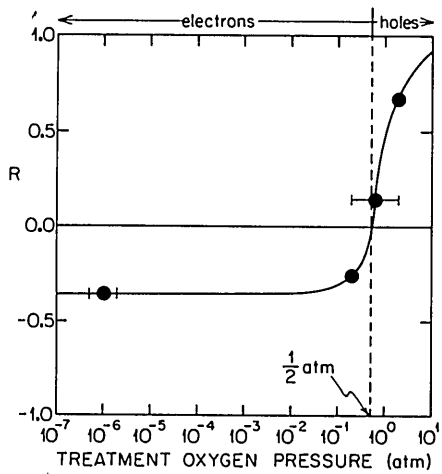

Fig. 10. The relative contribution R of hole and electron photoconduction [see Eq. (3d)] versus oxygen pressure during annealing. The effective oxygen pressure for the crystal as grown is unknown but is assumed to lie in the region indicated by the error bars, as discussed in the text. Note that R passes through zero at about ½ atm of O_2. The solid line is a qualitative guide.

Table 1. The Effective Density of Photorefractive Charge Carriers N_{pr}, the Relative Contribution of Hole and Electron Photoconduction R, and the Temperature of the Tetragonal-to-Cubic Phase Transition T_c for a Variety of $BaTiO_3$ Crystals

Crystal	N_{pr} ($\times 10^{16}$ cm^{-3})	R	T_c (°C)
[a] Rocky			
2.0 atm*	2.6	+0.67	126.3
as grown	0.6	0.14	—
0.2 atm*	1.1	−0.26	125.5
10^{-6} atm*	2.5	−0.36	120.0
[e] MMD			
as grown	0.5	0.24	—
treated in oil†	0.3	0.17	—
10^{-3} atm‡	1.0	+0.84	126
[b] Hop	1.9	+0.36	126
[c] Cat	6.2	+0.70	127
[d] Swiss	4.2	+0.89	128
[e] Doyle	4.1	+0.96	—

Experiments using these crystals are reported in [a] This study and Ref. 25, [b] Ref. 7, [c] Refs. 24 and 26, [d] Ref. 15. [e] Not previously reported.

* Oxygen partial pressure during treatment at 650°C for 36 h.

† Treated in Dow 200 Silohexane oil at 120°C for 72 h.

‡ Oxygen partial pressure during treatment at 550°C for 11 h.

F. Electron versus Hole Photoconduction

The electron and hole contributions to the photoconductivity (σ_+ and σ_-) were found to vary with the density of oxygen defects introduced into the $BaTiO_3$ crystal. Figure 10 is a plot of their relative contribution R [see Eq. (3d)] determined from the data of Fig. 8 versus the partial pressure of oxygen during treatment.[17,18] Electron photoconduction dominated after treatment with 10^{-6} atm or 0.2 atm of oxygen. Hole photoconduction dominated after treatment in 2.0 atm of oxygen.

Note that the crystal switches from electron-dominated to hole-dominated photoconduction at the same treatment oxygen pressure (~½ atm) at which the effective density N_{pr} of photorefractive charges is a minimum. This result is not required by the compensated semiconductor picture of Fig. 2 and may indicate an important aspect of the photorefractive effect not included here.

Table 1 is a summary of the measured density of photorefractive charges N_{pr} and the relative contribution R of holes and electrons for the crystal in this work (named Rocky) and a number of other $BaTiO_3$ crystals studied previously or in conjunction with this work. All crystals were melt grown by Sanders Associates.[19] Note that the experimentally determined values of R fall between −1 and +1, as predicted from Eq. (3d). Where measured, all these crystals as grown exhibited a photorefractive effect dominated by holes. Oxygen treatments at a lower temperature (550°C) were tried in a preliminary study on the $BaTiO_3$ crystal labeled MMD, with the results shown in Table 1. A further treatment of this sample at 650°C cracked the crystal, probably because it was heated and cooled too rapidly through its phase transition.

4. DISCUSSION: DONORS AND ACCEPTORS

Two pictures are useful in explaining our data. In the first picture oxygen vacancies are the photorefractive donors, and barium vacancies are the acceptors. Oxygen vacancies are known to be electron donors in $BaTiO_3$ at room temperature.[13,14] Barium vacancies are known to be electron acceptors with a thermal ionization enthalpy of 0.85 eV and occur naturally with a density of ~10^{17} cm^{-3}; the barium vacancy density is unchanged by treatments at 650°C in melt-grown $BaTiO_3$ crystals.[13] According to this picture, our oxidation and reduction treatments, which change the density only of oxygen vacancies and not barium vacancies, would alter the density of donors but not the density of acceptors.

A second picture has both the donors and the acceptors originating from a trace impurity, whose valence state can be altered by charge transfer with a nearby oxygen vacancy. In photorefractive $LiNbO_3$, for example, the donors are thought to be Fe^{2+} ions with an adjoining oxygen vacancy, and the acceptors are lone Fe^{3+} ions.[20] Previous studies with Fe-doped $BaTiO_3$ have shown that Fe can enter substitutionally for Ti^{4+} and that the Fe valence can be altered by charge transfer to an adjoining oxygen vacancy.[21] Recent evidence has shown that Fe is probably photorefractively active in $BaTiO_3$.[22] If so, then the oxidation/reduction treatments described here would have changed the densities of *both* the donor and the acceptor levels.

Both the above pictures are consistent with our data. One way of deciding between them would be to perform annealing experiments using an extremely low (~10^{-20}-atm) partial pressure of O_2, such as might be obtained by annealing in pure H_2.[21] According to the first picture above, this treatment would increase the density of donors (oxygen vacancies) without affecting the density of acceptors (barium vacancies) and would produce an effective charge density $N_{pr} = N_A$, as seen from Eq. (3c) above. However, according to the second picture above, treatment at very low oxygen pressure would cause all the acceptors to be converted to donors, making $N_{pr} = 0$.

5. PHOTOREFRACTIVE SPEED

The speed of the photorefractive effect was changed markedly by oxygen treatment. The photorefractive speed was

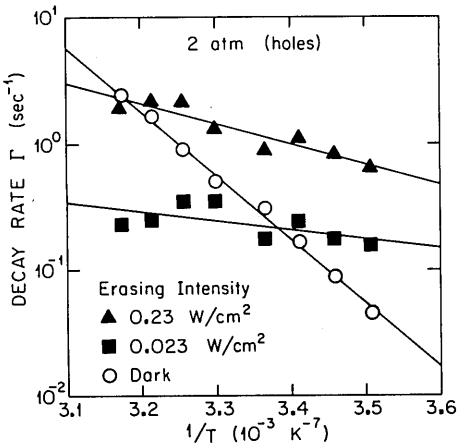

Fig. 11. The log of the light-induced grating decay rate (the dark decay rate has been subtracted) of the *heavily* oxidized $BaTiO_3$ crystal (O_2 treatment pressure 2.0 atm, *hole*-dominated photoconduction) versus inverse temperature of the crystal, for various light intensities: I_{erase} = 0.23 W/cm² (filled triangles); I_{erase} = 0.023 W/cm² (filled squares). The dark decay rate is also shown (open circles).

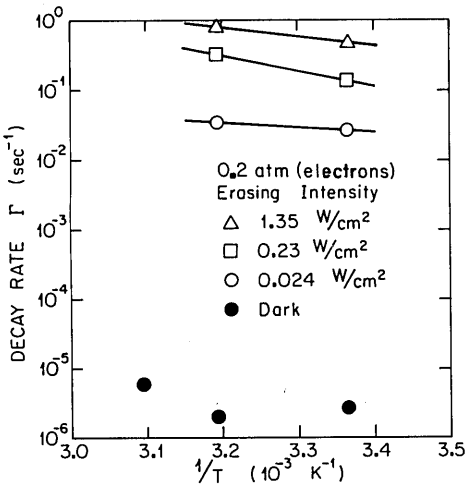

Fig. 12. The log of the grating decay rate of the reduced $BaTiO_3$ crystal (O_2 pressure during treatment 0.2 atm, *electron*-dominated photoconduction) versus inverse temperature of the crystal, for various light intensities: I_{erase} = 1.35 W/cm² (open triangles); I_{erase} = 0.23 W/cm² (open squares); I_{erase} = 0.024 W/cm² (open circles); dark erasure (filled circles).

measured by observing the decay of a photorefractive grating under uniform illumination, as described in detail in Ref. 23. The decay rate is [see Eq. (A10) of Appendix A]

$$\Gamma = [1 + (k/k_0)^2][\sigma_d + \sigma_+ + \sigma_-]/\epsilon\epsilon_0. \quad (9)$$

Here $\sigma_d \propto \exp(-T_0/T)$ is the *dark* conductivity and $(\sigma_+ + \sigma_-) \propto I^x$ is the total photoconductivity due to electrons and holes. The parameter T_0 is the activation energy (or thermal ionization enthalpy) of the acceptor sites, whereas the exponent x describes how the photoconductivity scales with the optical intensity.

A four-wave mixing geometry was used for the grating-erasure experiments.[7,23] Photorefractive gratings were first written with 3-mm-diameter optical beams, whose intensities were made unequal (I_1 = 0.005 W/cm² and I_2 = 0.1 W/cm²) in order to keep the modulation m small. A reading beam with a diameter of 3 mm and an intensity less than 1.0 $\times 10^{-6}$ W/cm² was incident counterpropagating to beam I_2. The reading-beam intensity was made so weak as to have no measurable effect on the grating erasure rate. The reading beam was Bragg deflected off the previously written photorefractive grating, and the diffraction efficiency was monitored with a photomultiplier tube and a digital storage system. With the writing beams turned off, the photorefractive grating was erased by a 1-cm-diameter optical erasing beam incident perpendicular to the plane of Fig. 4 with an intensity I_{erase} and an optical polarization along **k**. This erasing beam caused the diffraction efficiency of the photorefractive grating to decay and with a rate that increased with I_{erase}. All optical beams originated from the same argon-ion laser (operating at 514.5 nm on a single longitudinal TEM_{00} mode).

Figures 11 and 12 show the measured light-induced ($I_{erase} \neq 0$) and dark ($I_{erase} = 0$) grating erasure rates versus reciprocal temperature of the crystal. The temperature was varied over a 33°C range near room temperature. Figure 11 was obtained after the crystal had been treated in 2.0 atm of oxygen, which made *hole* transport dominant. The slope of the dark-decay-rate data of Fig. 11 yields an activation energy of T_0 = 11,400 K = 1.0 eV for dark erasure. This dark-erasure activation energy is the same as that measured in another crystal[23] of $BaTiO_3$ and is assumed to be the thermal ionization enthalpy of the photorefractive acceptors.

Figure 12 shows similar results obtained after the $BaTiO_3$ crystal was treated in 0.2 atm of oxygen, which made *electron* transport dominant. The dark-decay rate after this treatment was ~100,000 times smaller than the rates shown in Fig. 11. [The temperature dependence of this rate was not determined because the optical alignment tended to drift over the long time period (1 week) required to measure this rate.] A summary of the dark-decay rates at T = 24°C (after various treatments in oxygen) is 0.12 sec^{-1} (10^{-6} atm); ~3 $\times 10^{-6}$ sec^{-1} (0.2 atm); ~1 sec^{-1} (as grown); 0.31 sec^{-1} (2.0 atm).

The light-induced decay rate $[(\sigma_+ + \sigma_-)/\epsilon\epsilon_0$ in Eq. (10)] showed a weak temperature dependence for both hole-dominated photoconduction, as seen in Fig. 11, and electron-dominated photoconduction, as seen in Fig. 12.

Oxygen treatment also caused a marked variation in the dependence of photorefractive speed on optical intensity. Figure 13 is a plot of the light-induced erasure rate versus erasing intensity for the electron-dominated and hole-dominated cases. Electron photoconduction dominated after the crystal was treated in 10^{-6} atm of oxygen, and the speed increased linearly with optical intensity (speed $\propto I^1$). After the crystal was treated at the higher oxygen pressures the speed increased sublinearly with optical intensity (speed $\propto I^x$) whether electron or hole photoconduction dominated. The value of the exponent was x = 0.76 after treatment at 0.2 atm of oxygen (electrons) and x = 0.67 after treatment with 2.0 atm of oxygen (holes). This sublinear intensity dependence of the decay rate in the present $BaTiO_3$ crystal and in two crystals previously studied[23,24] has not yet been explained. (Both the band-conduction model and the hopping model predict a decay rate that increases linearly with intensity.)

The fact that a $BaTiO_3$ sample reduced in 10^{-6} atm of oxygen responds *linearly* with optical intensity is of practical importance, for it implies that high-speed operation of a

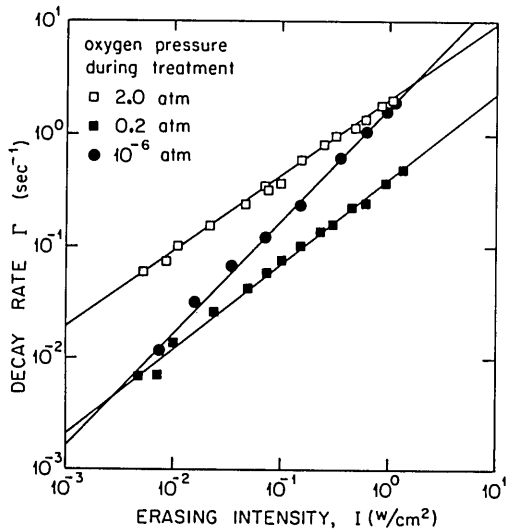

Fig. 13. The grating decay rate versus light intensity, for various oxygen partial pressures during treatment: 2 atm (open squares); 0.2 atm (filled squares); 10^{-6} atm (filled circles). The crystal temperature was held at $T = 24°C$ for these experiments, and the grating wave vector was $k = 0.2\ (n\omega/c)$.

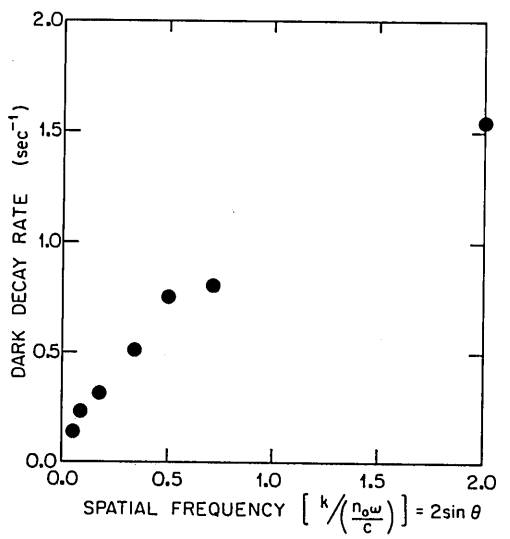

Fig. 14. The dark-decay rate versus grating spatial frequency in the $BaTiO_3$ crystal after treatment in 2-atm oxygen (hole conduction). $T = 24°C$ during these experiments.

photorefractive device using this sample could be achieved with less optical intensity than in the oxidized samples, where the speed increases *sublinearly* with optical intensity. Figure 13 shows that for the highly reduced sample, which has a linear photoconductivity, about 1 J/cm^2 is required for a $1/e$-fold grating erasure, independent of intensity. This linearly extrapolates to 1-nsec operation at an optical intensity of 1 gW/cm^2. Sublinear extrapolation for the heavily oxidized $BaTiO_3$ sample predicts that an optical intensity 1000 times larger would be needed to obtain the same speed and would surely cause optical damage to the crystal.

Figure 14 shows the dependence of the dark-erasure rate on grating spatial frequency at $T = 24°C$ for the sample that had been treated in 2.0 atm of oxygen. The parabolic shape predicted by Eq. (8) and observed in Ref. 7 is not observed and suggests that the hopping distance may be comparable to the grating spacing, as discussed in Ref. 11.

6. CONCLUSION

A $BaTiO_3$ single crystal was treated in several different oxygen atmospheres to create or fill oxygen vacancies. The partial pressure of oxygen during treatment determined the effective density of photorefractive charge carriers. The relative contributions of electron and hole photoconduction were also altered by the treatments; hole photoconduction dominated at high oxygen partial pressures and electron photoconduction dominated at low oxygen partial pressures. The oxygen vacancies (or complexes composed of an oxygen vacancy adjacent to an impurity) are shown to be the photorefractive donors of negative charge, as supported by measurements of the transition temperature and the optical absorption spectra. $BaTiO_3$ exhibited a sublinear photoresponse when used as grown or when treated at higher oxygen partial pressures (i.e., when oxidized). However, $BaTiO_3$ exhibited a linear photoresponse after treatment at an oxygen partial pressure of 10^{-6} atm (a reducing atmosphere). This linear photoresponse will make it easier to achieve high-speed operation of photorefractive $BaTiO_3$ devices with less optical intensity.

APPENDIX A

Here we generalize the hopping equations of Ref. 7 to include both electron and hole photoconduction and also to allow site occupation probabilities W_n that are not necessarily small. The probability that the nth site is occupied by an electron changes with time according to

$$\begin{aligned} dW_n/dt = + \sum_{m\neq n} D^h{}_{nm}[&(1 - W_n)W_m I_n \exp(+\beta\varphi_{nm}/2) \\ &- (1 - W_m)W_n I_m \exp(+\beta\varphi_{mn}/2)] \\ - \sum_{m\neq n} D^e{}_{nm}[&W_n(1 - W_m)I_n \exp(-\beta\varphi_{nm}/2) \\ &- W_m(1 - W_n)I_m \exp(-\beta\varphi_{mn}/2)]. \end{aligned} \tag{A1}$$

The first sum accounts for holes hopping, and the second sum for electrons hopping. Here, as in Ref. 7, n is the site located at position r_n, W_n is the probability that an electron occupies site n, $1 - W_n$ is the probability that a hole occupies site n, $D^e{}_{mn}$ is the electron hopping rate coefficient between sites n and m, $D^h{}_{mn}$ is the hole hopping rate coefficient between sites n and m, $\varphi_{nm} = \varphi_n - \varphi_m$, where φ_n is the electrostatic potential at site n, I_n is the optical intensity at site n, and $\beta = e/k_BT$. (Note: $e > 0$ is the absolute magnitude of the electron or hole charges.)

Consider an optical illumination that varies sinusoidally according to

$$I_n = I_0\{1 + \mathrm{Re}[m \exp(ikz_n)]\}, \tag{A2a}$$

where m is the complex intensity modulation (before the buildup of any space-charge field). We consider the case of a small intensity modulation ($|m| \ll 1$), so that we can ignore terms having a spatial variation other than $\exp(ikz_n)$, and try solutions of the form

$$W_n \equiv W_0\{1 + \mathrm{Re}[w \exp(ikz_n)]\}, \tag{A2b}$$

$$\varphi_n \equiv \mathrm{Re}[\varphi \exp(ikz_n)], \tag{A2c}$$

where $|w|$ and $|\beta\varphi|$ will both be small compared to unity. Equation (A2c) assumes that there is no applied or intrinsic spatially uniform electric field.

If the density of electron donors exceeds that of acceptors $N_D > N_A$, then the average probability that a site is occupied by an electron will be $W_0 = 1 - N_A/N_D$, and the total number of sites will be $N = N_D$. If the density of electron acceptors exceeds that of donors $N_A > N_D$, then the average probability that the site is occupied by an electron is $W_0 = N_D/N_A$, and the total number of sites will be $N = N_A$.

Poisson's equation yields

$$\varphi = (W_0 w N e)/(\epsilon\epsilon_0 k^2), \tag{A3}$$

where N is the average density of sites. Keeping only those terms in Eq. (A1) that are of first order in the small quantities m and w:

$$dw/dt = -I_0 k_0{}^2 l^2 [w(D_e + D_h)(1 + k^2/k_0{}^2) + m(D_e - D_h)(1 - W_0)(k^2/k_0{}^2)], \tag{A4}$$

where $k_0{}^2 \equiv [e^2 W_0(1 - W_0)N]/(\epsilon\epsilon_0 k_B T)$ and D^e and D^h are the effective hopping rate constants, which depend on the explicit form of the hopping probabilities, $D^e{}_{mn}$ and $D^h{}_{mn}$.

For nearest-neighbor hopping between sites separated by an average distance $l = N^{-1/3}$, the hopping rate coefficient $D^e{}_{mn} = 0$ except for $m = n \pm 1$, in which case $D^e{}_{mn} = D_0{}^e$, and the summation over m gives

$$D^e = 2D_0{}^e[1 - \cos(kl)], \tag{A5a}$$

with a similar term for holes.

Another possibility is that the hopping is long range, extending over many sites, with an exponentially decreasing probability and with an average hopping distance $1/\kappa_e \gg l$.[11] For this case $D^e{}_{mn} = D_0{}^e(1/\kappa_e r)\exp(-\kappa_e r)$ for electrons. Approximating the sum over m by a three-dimensional integral,[11]

$$D^e = D_0{}^e(4\pi N/\kappa_e{}^3)[(k/\kappa_e)^2/(1 + (k/\kappa_e)^2)], \tag{A5b}$$

with a similar result for holes.

In the limit $kl \ll 2\pi$ in Eq. (A5a) and $k \ll \kappa$ in Eq. (A5b), both equations reduce (within a constant factor) to $D^e \approx D_0{}^e(kl)^2$, and Eq. (A4) becomes

$$dw/dt = -[I_0(D_e + D_h)(k_0 l)^2 + \Gamma_d]\{w[1 + (k/k_0)^2] + mR(k/k_0)^2\}, \tag{A6}$$

where $R = (D_h - D_e)/[(D_h + D_e) + \Gamma_d/(I_0 k_0{}^2 l^2)] = (\sigma_+ - \sigma_-)/(\sigma_+ + \sigma_- + \sigma_d)$ in terms of conductivities $\sigma_\pm = I_0 D_{h,e}(k_0 l)^2 \epsilon\epsilon_0$. The dark, or thermal, conductivity (σ_d) has been included in the final result and is analogous to the unmodulated part of the incident illumination (I_0).

In the steady state, $dw/dt = 0$, and Poisson's equation gives

$$E_{sc} = -iwW_0 eN_{pr}/k\epsilon\epsilon_0 = i(k_B T/e)Rmk/[1 + (k/k_0)^2], \tag{A7}$$

$$N_{pr} = N_A(1 - N_A/N_D) \text{ if } N_A < N_D \tag{A8}$$

$$= N_D(1 - N_D/N_A) \text{ if } N_D < N_A.$$

If $m = 0$ (uniform illumination) and $|w| > 0$, the grating will decay with a rate Γ:

$$dw/dt = -\Gamma w, \tag{A9}$$

where the grating erasure rate is

$$\Gamma = [I_0(D_e + D_h)(k_0 l)^2 + \Gamma_d][1 + (k/k_0)^2]. \tag{A10}$$

ACKNOWLEDGMENTS

We thank R. W. Boyd of the University of Rochester and M. M. Tehrani of the Honeywell Corporation for the generous use of their $BaTiO_3$ samples. This work was supported by the U.S. Air Force Office of Scientific Research under contract no. F49620-85-0110 and the Joint Services Electronics Program under contract no. F49620-85-C-0071.

REFERENCES AND NOTES

1. J. Feinberg, "Optical phase conjugation in photorefractive materials," in *Optical Phase Conjugation*, R. A. Fisher, ed. (Academic, New York, 1983), Chap. 11 and references therein.
2. J. Feinberg, "Real-time edge enhancement using the photorefractive effect," Opt. Lett. **5,** 330–332 (1980).
3. J. Feinberg and R. W. Hellwarth, "Phase-conjugating mirror with continuous-wave gain," Opt. Lett. **5,** 519–521 (1980); Erratum: Opt. Lett. **6,** 257 (1981).
4. J. O. White, M. Cronin-Golomb, B. Fischer, and A. Yariv, "Coherent oscillation by self-induced gratings in the photorefractive crystal $BaTiO_3$," Appl. Phys. Lett. **40,** 450–452 (1982).
5. W. B. Whitten and J. M. Ramsey, "Self-scanning of a dye laser due to feedback from a $BaTiO_3$ phase-conjugate reflector," Opt. Lett. **9,** 44–46 (1984).
6. J. Feinberg and G. D. Bacher, "Self-scanning of a continuous-wave dye laser having a phase-conjugating resonator cavity," Opt. Lett. **9,** 420–422 (1984).
7. J. Feinberg, D. Heiman, A. R. Tanguay, Jr., and R. W. Hellwarth, "Photorefractive effects and light-induced charge migration in barium titanate," J. Appl. Phys. **51,** 1297–1305 (1980); erratum: J. Appl. Phys. **52,** 537 (1981).
8. N. V. Kukhtarev, V. B. Markov, S. G. Odulov, M. S. Soskin, and V. L. Vinetskii, "Holographic storage in electrooptic crystals. I. Steady state," Ferroelectrics **22,** 949–960 (1979).
9. R. Orlowski and E. Kratzig, "Holographic method for the determination of photo-induced electron and hole transport in electro-optic crystals," Solid State Commun. **27,** 1351–1354 (1978).
10. M. B. Klein and G. C. Valley, "Beam coupling in $BaTiO_3$ at 442 nm," J. Appl. Phys. **57,** 4901–4905 (1985).
11. R. A. Mullen and R. W. Hellwarth, "Optical measurement of the photorefractive parameters of $Bi_{12}SiO_{20}$," J. Appl. Phys. **58,** 40–44 (1985).
12. For the case $N_A > N_D$, because the donor level is far removed from the valence band, we assume that the recombination rate of electrons in the donor level with holes in the valence band is much larger than any process that tends to fill the donor level.
13. A. M. J. H. Seuter, "Defect chemistry and electrical transport properties of barium titanate," Philips Res. Rep. Suppl. **3,** 1–84 (1974).
14. S. Ikegami and I. Ueda, "Semiconductive single crystal of $BaTiO_3$ reduced in a hydrogen atmosphere," J. Phys. Soc. Jpn. **19,** 159–166 (1964).
15. K. R. MacDonald, J. Feinberg, M. Z. Zha, and P. Gunter, "Asymmetric transmission through a photorefractive crystal of barium titanate," Opt. Commun. **50,** 146–150 (1984).
16. This value of $r_{13} = 14 \times 10^{-12}$ m/V was measured by the authors on two similar crystals of melt-grown $BaTiO_3$ using a Mach–Zehnder interferometer with the crystal in one arm, applying a 100-V/cm dc field along the c axis, and then adding an additional ac field of 20 V/cm (peak to peak) at frequencies ranging from 10 Hz to 100 kHz. These measurements will be described in more detail in a future publication.
17. Because the sign of R has been positive in nearly all crystals as grown (including the results summarized in Table 1 and, with one exception, the crystals studied in Ref. 10), we assume that our as-grown crystal had a positive R.

18. If the crystal were only partially poled, and contained invisible 180° domains (90° domains would have been clearly visible), then the effective Pockels coefficient r_{eff} would be reduced. This would produce an incorrect value for $|R|$. To verify that the crystal was completely poled by our poling method, we measured R, repeated the poling using twice the usual applied electric field, and remeasured R, which was unchanged. We therefore assume that the crystal was fully poled by our technique.
19. A. Linz, V. Belruss, and C. S. Naiman, J. Electrochem. Soc. **112**, 60C (1965).
20. G. E. Peterson, A. M. Glass, and T. J. Negran, "Control of the susceptibility of lithium niobate to laser-induced refractive index changes," Appl. Phys. Lett. **19**, 130–132 (1971); W. Phillips and D. L. Staebler, "Control of the Fe^{2+} concentration in iron-doped lithium niobate," J. Elec. Mater. **3**, 601–617 (1974).
21. H. J. Hagemann, A. Hero, and U. Gonser, "The valance change of Fe in $BaTiO_3$ studied by Mössbauer effect and gravimetry," Phys. Status Solidi **61**, 63–72 (1980). At high oxygen-treatment pressures (~1 atm) Fe^{4+} was predominant; in crystals as grown and after treating at $\sim 10^{-4}$ atm Fe^{3+} was predominant; after treating at 10^{-26} atm, the fraction of Fe^{2+} became significant.
22. M. B. Klein, "Origins of the photorefractive effect in $BaTiO_3$," Proc. Soc. Photo-Opt. Instrum. Eng. **519**, 136–141 (1984).
23. S. Ducharme and J. Feinberg, "Speed of the photorefractive effect in a $BaTiO_3$ single crystal," J. Appl. Phys. **56**, 839–842 (1984).
24. L. K. Lam, T. Y. Chang, J. Feinberg, and R. W. Hellwarth, "Photorefractive-index gratings formed by nanosecond optical pulses in $BaTiO_3$," Opt. Lett. **6**, 475–477 (1981).
25. S. Ducharme and J. Feinberg, "Control of the density of photorefractive charge carriers in $BaTiO_3$ single crystals," J. Opt. Soc. Am. A **1**, 1213 (A) (1984).
26. J. Feinberg, "Self-pumped, continuous-wave phase conjugator using internal reflection," Opt. Lett. **7**, 486–488 (1982).